The position of the midlatitude storm track and eddy-driven westerlies in aquaplanet AGCMs

Jian Lu[1,2] Gang Chen[3] Dargan M. W. Frierson[4]

[1]Center for Ocean-Land-Atmosphere Studies, Institute of Global Environment and Society, Calverton, MD

[2]Department of Atmospheric, Oceanic and Earth Sciences, George Mason University, Fairfax, VA

[3]Department of Earth and Atmospheric Sciences, Cornell University, Ithaca, NY

[4]Department of Atmospheric Science, University Washington, Seattle, WA

Corresponding author: Jian Lu, Center for Ocean-Land-Atmosphere Studies, 4041 Powder Mill Rd, Suite 302, Calverton, MD, 20705-3106. E-mail: jianlu@cola.iges.org

Abstract

The sensitivity of the midlatitude storm track and eddy-driven wind to the sea surface temperature (SST) boundary forcing is studied over a wide range of perturbations using both simple and comprehensive general circulation models over aquaplanet lower boundary conditions. Under the single-jet circulation regime similar to the conditions of the present climate in the Northern Hemisphere winter or the Southern Hemisphere summer, the eddy-driven jet shifts monotonically poleward with both the global mean and the equator-to-pole gradient of the SST. The eddy-driven jet can have a reverse relationship to the gradient if it is well-separated from the subtropical jet and Hadley cell boundary in a double-jet circulation regime.

A simple scaling is put forward to interpret the simulated sensitivity of the storm track/eddy driven westerly wind position within the single-jet regime in both models. The rationale for the scaling is based on the notion that the wave activity flux can propagate horizontally away from the source region resulting in a broader distribution of eddy potential vorticity (PV) flux in the upper troposphere than that of an opposite sign in the lower troposphere and, as a consequence, the position of the maximum of the eddy-driven westerlies tends to be controlled by the profile of the relatively sharp-peaked low-level PV flux, which is dominated by the eddy heat flux component of the Eliassen-Palm (EP) flux. Thus, the position of the eddy driven surface westerlies may be inferred from the vertical EP flux coming out of the lower troposphere. The vertical EP flux can be parameterized by a measure of baroclinicity, whose latitudinal variations show a linear relationship with the meridional displacement of the eddy-driven westerlies and the storm track. This relationship still holds well within the single-jet regime even when only the variation of static stability is taken into consideration in estimating the baroclinicity (the temperature gradient component of which is fixed). To the extent that the static stability is

deterministically constrained by and hence can be predicted from the given SST conditions through a moist scaling for the midlatitude stratification, one may, given SST perturbations, predict which way the storm track and eddy driven wind should shift with respect to a chosen reference climate state. The resultant anomaly-wise scaling turns out to be valid for both the idealized and comprehensive models, regardless of the details in the model physics.

By corollary, it can be argued that the poleward shift of storm track found in the global warming simulations by fully coupled climate models may be attributed, at least partially, to the increase in the subtropical and midlatitude static stability with global warming.

1. Introduction

Most of the midlatitudes are under the influence of the storm tracks. The dynamics of storm tracks has been the central theme of climate dynamics, inspiring numerous studies (e.g., Hartmann 1974; Blackmon 1976; Blackmon et al., 1977; Hoskins et al., 1989; Hoskins and Valdes, 1990; Chang 2001; Chang et al., 2002; Bengttson, et al., 2006). The storm tracks have a conspicuous seasonal cycle in their locations: they shift equatorward in step with the jet stream from fall to midwinter, and then migrate poleward afterwards (Hoskins et al., 1989; Nakamura, 1992). In addition, at interannual time scales, ENSO can impact the latitudinal position of the storm track and the jet stream, with the warm phase leading to an equatorward contraction (Robinson, 2002; Seager et al., 2003; Orlanski, 2005; L'Heureux and Thompson 2006; Lu et al., 2008; Chen et al. 2008; Brayshaw et al., 2008) and vice versa. The issue of the latitudinal position of the storm track and jet stream shift is particularly topical given that the poleward shift of the mid-latitude storm tracks is deemed to be one of the most robust predicted features under global warming (e.g., Kushner et al., 2001; Yin, 2005; Lorenz and DeWeaver, 2007; Lu et al., 2008; Chen et al., 2008). Nevertheless, the mechanistic research on the storm track has hitherto been largely focused on the intensity (e.g., James, 1987; Chang, 2001; Nakamura, 1992; Straus and Shukla, 1988), and much is yet to be learned as to the mechanisms that control the location of the storm track.

Hoskins and Valdes (1990) perceived the storm track as being *self-maintaining* in the sense that storm track eddies in general are most vigorous downstream of the region of peak baroclinicity, and the mixing of temperature by eddies is relatively benign where the baroclinicity is largest. Further, the enhanced baroclinicity over the storm track entrance region is actively maintained by condensational heating, which in turn is caused by the cyclones

themselves. The self-maintaining nature of the storm track implies that the transient component and the mean flow (and the associated thermal structure) are just integral parts of the same phenomenon: the storm track will always ensure that the baroclinicity is locally maximum nearby. The classic theory of linear baroclinic instability states that eddies grow by tapping the background available potential energy (e.g., Eady, 1949; Charney, 1947; Phillips, 1954) and thus one may argue that the storm track is excited by the mean flow baroclinicity. Some have attempted to explain the shift of eddy field by a measure of mean baroclinicity such as the Eady Growth Rate (e.g., Inatsu et al., 2003; Brayshaw et al., 2008). The linear baroclinic instability theory no doubt has its value in understanding the existence of the storm track; however, in many cases one has to explain where the mean baroclinicity or the variation thereof comes from in the first place. As will be shown later for the cases considered in the current study, the baroclinicity evaluated based on the mean temperature in radiative-convective equilibrium gives little clue as to which way the storm track should move, whereas, the latitudes of the maxima of eddy statistics do vary in tandem with the mean wind when eddy adjustment is taken into account in the maintenance of the mean temperature.

In this study, we will use the *eddy-driven surface westerly* (EDSW) as the proxy for the storm track. The EDSW, as the term implies, results from the balance between the vertically integrated eddy momentum convergence and the surface drag; and the surface drag acting on it is locally balanced by the Coriolis force associated with the poleward flow at the bottom of the Ferrel cell. Thus, intuitively, the maximum EDSW can be used as a proxy for the position of the storm track and any predictive power obtained for the westerly wind can potentially be carried over to the other properties of the midlatitude storm track.

It is beyond the scope of the present study to construct a rigorous closure theory for the storm track; our goal instead is to strive for the most primary dynamic factors that can be used to infer the movement of the storm track proxy—the EDSW. The most important attribute of these factors should be that they are quantifiable from the conditions given for the problem, such as the Sea Surface Temperatures (SSTs), so that through them one might be able to link the variation in the position of the storm track/EDSW to the given conditions. This exercise, which will be referred to as scaling for convenience, will be carried out for a suite of aquaplanet model simulations with two distinct GCMs under the same prescribed SST boundary conditions. If the proposed scaling can be validated, it should help shed light on the key processes that are responsible for the shift of the storm track/EDSW under different climate conditions. Two GCMs with distinct physics and parameterizations are used here to assess the robustness of our scaling.

The whole endeavor is also motivated by the observation that the best-measured quantity in both modern and paleo-climate records is the surface temperature, and one may potentially tap into this resource by forming a heuristic relationship that links surface temperature to the midlatitude mean flow and eddy statistics. Any success along this line may lead to some predictive power for the changes of storm track in the past and future.

The models and experiments will be detailed in Section 2. Model simulations of the storm tracks and the EDSW will be reported in Section 3. Section 4 lays out the rationale of the scaling, which is to be validated in Section 5. Finally we conclude with summary and discussion on the possible implications for climate change in the past and future.

2. Model Description and Simulations

2a. Idealized GCM

The idealized GCM is an ice-free, land-free model (or so-called aquaplanet model) consisting of various simplified physical parameterizations coupled to a spectral dynamical core that solves the primitive equations (Frierson et al., 2006; Frierson 2007a). For longwave radiative transfer, a gray scheme is used with fluxes that are a function only of temperature, and not of water vapor or other constituents. Water vapor itself is a prognostic variable, but there is no liquid water or clouds. Condensation and moist convection is represented by a simplified version of the Betts-Miller convection scheme (Betts, 1986; Betts and Miller, 1986; Frierson 2007a) and a grid-scale condensation scheme. The simplified model physics also includes a simplified Monin-Obukhov surface flux scheme, and a K-profile boundary layer scheme. All simulations in this study are run at a resolution of T42 in the horizontal, and 25 levels in the vertical.

2b. Full GCM

The full GCM simulations in this paper are the same simulations originally used to study poleward heat transports in the study of Caballero and Langen (2005). The model is a comprehensive GCM, with full representations of clouds, radiation, convection, and other physics. The atmospheric model used for these simulations is the Parallel Community Climate Model Version 3 (PCCM3), which is the atmospheric component of the Fast Ocean-Atmosphere Model (FOAM) (Jacob 1997). The model uses the physical parameterizations of the NCAR CCM3.6 model (Kiehl et al. 1996) and the dynamical core of the NCAR CCM2 model. The full GCM is run at T42 resolution, with 18 vertical levels. Sea ice is specified where SST is below 0°C.

2c. Boundary conditions

The boundary conditions used here are from the study of Caballero and Langen (2005). The solar insolation is set to be a perpetual equinoctial condition. The surface is an aquaplanet with

no topography, and prescribed, zonally symmetric SST distributions. The SSTs are functions of latitude (ϕ) only

$$T_s(\phi) = T_m - \Delta T(3\sin^2\phi - 1)/3, \qquad (1)$$

controlled by two parameters: T_m is the global mean temperature, ΔT is the equator-to-pole temperature difference. The functional form is chosen so that changes in ΔT result in no net change in global mean temperature and the maximum gradient is always located at 45° latitude. We examine simulations with T_m ranging between 0 and 35°C, and ΔT between 10° and 60°C. For the idealized model, simulations are run at 10°C increments for T_m and ΔT, with additional runs of T_m = 35°C; for the full GCM experiments, simulations are conducted for every 5°C intervals over the same parameter range except the few cases that the tropical SST is too warm to be relevant. It should be noted that due to the functional form of (1), the tropical temperatures increase with increases in both mean temperature and temperature gradient. All simulations are spun up for 1 year, and statistics are calculated over 3 subsequent years of integration. The time mean fields are calculated by averaging the Northern and Southern Hemispheres since the prescribed SST and the resulting model climatology are hemispherically symmetric.

3. Results of Model Simulations

We first examine the EDSW position in the suite of simulations with the two models. As shown in Figure 1c, the axis of storm track (measured as vertically integrated Eddy Kinetic Energy, EKE) is in excellent alignment with the latitude of the maximum EDSW in the idealized model simulations. To a lesser extent, this relationship also holds for the full GCM (Figure 1d). In general, it is justifiable that the shift of the EDSW is representative of that of the EKE of the storm track, with some cautionary discretion applied to the full model. This result, in a context of

our aquaplanet simulations, corroborates the notion that mean wind moves in concert with the transients.

Both the idealized and full GCMs simulate a monotonic poleward shift of the EDSW/storm track with increasing global mean temperature T_m — probably the most robust feature in all the simulations[1]. Another robust feature, not shown, is the intensification of storm activity and the EDSW with increasing SST gradient ΔT (see Figure3a in Caballero and Langen, 2005). However, the two GCMs show a distinct difference in the sensitivity of the storm track/EDSW position to ΔT. For the idealized model, the position of the EDSW is also a monotonic function of ΔT, moving poleward with increasing ΔT. This is not the case for the full GCM. In the middle of the T_m-ΔT space, as ΔT increases from its lowest value, the EDSW first shifts equatorward, and then poleward after passing its most equatorial position at the intermediate value similar to the conditions of present climate. The distinct behavior between the two models rules out a possible unifying scaling theory for the position of storm track/EDSW valid for the whole range of SST parameters and for both models. Therefore, in this study we will only strive for an anomaly-wise scaling for the anomalous shift of EDSW due to perturbations with respect to a certain chosen reference state.

Further inspection on the zonal wind profiles of the full GCM suggests that this peculiar phenomenon of an equatorward shift with ΔT may be related to the large separation between the subtropical jet and eddy-driven jet when the global mean SST is warm but the SST gradient is weak (the upper left domain in Figure 1b). These cases with a zonal wind profile characterized by a distinct split-jet condition are marked with crosses in Figure 1b. It is worth noting that the

[1] In a set of simulations with a similar idealized GCM over an extended range of climate forcing (Schneider et al., 2010), the surface westerlies actually move equatorward with warming over part of the range of the simulations despite the fact that the heat flux and near surface EKE move poleward—an interesting counter example to the cases studied here.

wind profiles in the split-jet regime bear a strong resemblance to those of the bifurcation discussed by Lee and Kim (2003) and Chen and Plumb (2009). In the case of Lee and Kim (2003), the bifurcation occurs when the subtropical jet is intensified by equatorial heating and as a result, the midlatitude disturbances are more subject to the waveguiding effect of a stronger subtropical jet (which itself is stable in position) and hence shift equatorward. The sharp regime transition toward a merged jet at ~30° latitude never takes place in our case. Rather, the eddy-driven jet merely progresses gradually equatorward as the subtropical jet grows in strength with increasing ΔT. As ΔT approaches its middle range, the eddy-driven jet and the subtropical jet start to merge, and a different mechanism begins to come into play in the response of EDSW position to ΔT — a subject of focus of the present scaling study to be elaborated in the following sections. A typical transition from split- to single-jet regime in the full GCM with increasing ΔT is exemplified by Figure 2, which shows the profiles of 400 hPa zonal wind for the cases of T_m=15°C, with ΔT varying from 10 to 50°C at increments of 5°C.

4. Rationale for scaling

The rationale of this rather empirical scaling is based on the understanding of a two-layer quasi-geostrophic (QG) model for the midlatitude dynamics: the meridional structure of the lower tropospheric wind is shaped by the vertically integrated eddy potential vorticity flux (Robinson 2000, 2006; Pavan and Held, 1996), i.e.,

$$\overline{u}_2 = \frac{1}{\kappa}\left(\mathcal{F}_1 + \mathcal{F}_2\right) \tag{2}$$

where the overbar denotes zonal mean; κ represents the rate of a frictional damping on the lower level velocity; $\mathcal{F}_i = \overline{(v_i' q_i')}$ are the zonally averaged eddy fluxes of QG potential vorticity

(PV) with subscript *i*=1, 2 indicating the upper and lower troposphere, respectively. Under the QG approximation, these are equivalent to the divergence of the Eliassen-Palm (EP) fluxes on both levels (Edmon et al., 1980), so that $\mathcal{F}_2$, which is typically positive in the real atmosphere, may be considered the source of Eliassen-Palm eddy activity, while $\mathcal{F}_1$ may be considered its dissipative sink aloft. In applying this framework to a continuously stratified atmosphere, we use the vertical integration over levels above and below 560 hPa to estimate the eddy fluxes for the upper (1) and lower (2) troposphere, respectively. With the atmosphere so partitioned, and with the QG EP flux defined as

$$\mathbf{F} \equiv (-\overline{u'v'})\mathbf{j} + \left(\frac{f\,\overline{v'\theta'}}{\bar{\theta}_p} \right)\mathbf{k} \ ,$$

where **j** and **k** are the unit vectors pointing northward and upward, respectively and other symbols carry their conventional meaning, the eddy PV fluxes ($\mathcal{F}_i$) and its components of associated momentum flux convergence ($\mathcal{M}_i$) and heat fluxes ($\mathcal{H}_i$) can be expressed as

$$\mathcal{F}_1 \equiv \frac{1}{p_s} \int_{p=560}^{p=0} \nabla \cdot \mathbf{F}\, dp = \mathcal{M}_1 + \mathcal{H}_1 \tag{3a}$$

$$\mathcal{F}_2 \equiv \frac{1}{p_s} \int_{p=p_s}^{p=560} \nabla \cdot \mathbf{F}\, dp = \mathcal{M}_2 + \mathcal{H}_2 \tag{3b}$$

where

$$\mathcal{M}_1 = \frac{1}{p_s} \int_{p=560}^{p=0} dp \left\{ \frac{\partial}{\partial y}(-\overline{u'v'}) \right\},$$

$$\mathcal{H}_1 = \frac{1}{p_s} \int_{p=560}^{p=0} \frac{\partial}{\partial p}\left(\frac{f\,\overline{v'\theta'}}{\bar{\theta}_p} \right) dp = -\frac{1}{p_s} \left. \frac{f\,\overline{v'\theta'}}{\bar{\theta}_p} \right|_{p_{560}} ,$$

$$\mathcal{M}_2 = \frac{1}{p_s} \int_{p=p_s}^{p=560} dp \left\{ \frac{\partial}{\partial y}(-\overline{u'v'}) \right\},$$

and

$$\mathcal{H}_2 = \frac{1}{p_s}\int_{p=p_s}^{p=560} \frac{\partial}{\partial p}\left(\frac{f\,\overline{v'\theta'}}{\overline{\theta}_p}\right)dp = \frac{1}{p_s}\frac{f\,\overline{v'\theta'}}{\overline{\theta}_p}\bigg|_{p_{560}} \qquad (4)$$

A boundary condition of no perturbation has been applied to $p = 0$ in the expression of $\mathcal{H}_1$ and to $p = p_s$ in the expression of $\mathcal{H}_2$. Note that this treatment of bottom boundary condition is conceptually consistent with the generalization of Bretherton (1966), in which a PV sheet associated with a concentrated PV gradient is inserted at an infinitesimal distance from the boundary, as such the eddy PV flux **F** can be taken to be zero at the boundary (p_s) but non-zero immediately away from the boundary (p_s^-).

Observations (Edmon et al., 1980) demonstrate that the meridional structure of the vertically integrated PV flux ($\mathcal{F}_1 + \mathcal{F}_2$) near the latitude of the maximum surface wind is dominated by the low level flux ($\mathcal{F}_2$), which is in turn dominated by the heat flux component ($\mathcal{H}_2$). Figure 3 depicts the meridional profiles for upper tropospheric PV flux $\mathcal{F}_1$ (blue), upper tropospheric momentum flux convergence $\mathcal{M}_1$ (dashed black), lower tropospheric PV flux $\mathcal{F}_2$ (red) and associated heat flux component $\mathcal{H}_2$ (red dashed), all normalized by the maximum of $\mathcal{F}_2$, and the surface wind (U_s, black) for the whole suite of simulations (except the cases of $\Delta T = 10$) with the idealized model. With increasing SST gradient and hence increasing intensity of the transient activity, the meridional structure of the surface wind tends to be increasingly shaped by $\mathcal{F}_2$ near the peak, which is in turn dictated by that of $\mathcal{H}_2$ (as one can see by comparing the two red curves in Figure 3). With increasing SST gradient, there is also an increasing tendency for the heat flux ($\mathcal{H}_1$ or negative $\mathcal{H}_2$) and the momentum flux ($\mathcal{M}_1$) components in the upper level to cancel with each other. It is particularly worth noting that across all the SST cases there is an inclination for

the peak of the upper level momentum flux convergence $\mathcal{M}_1$ (hence the eddy-driven surface westerly wind) and the peak of $\mathcal{H}_2$ to move in tandem latitudinally, although their peaks do not always coincide. To the extent that the variation of the $\mathcal{H}_2$ is implicative of the movement of the EDSW, if the former can be predicted based on the conditions provided, from which one may be able to infer the direction of the shift of the EDSW and the storm tracks. To do so, we first parameterize $\mathcal{H}_2$ in terms of a quantity that is a function of the mean (temperature) field, which could potentially be deduced from the SST boundary conditions; the shift of the parameterized quantity (with respect to a chosen reference state) predicted from SST can then be used to indicate the shift of the EDSW. To make this approach most relevant to the current climate, we choose the case [T_m=20°C, ΔT =40°C] as the reference state.

We first parameterize the eddy heat flux. Given that the lower tropospheric finite amplitude eddy production is fundamentally local and hence effectively diffusive, the eddy-induced heat flux may be related to the local mean temperature gradient in form of $\overline{v'\theta'} = -\mathcal{D}\frac{\partial\bar{\theta}}{\partial y}$. With not much discretion assigned to the specific form of the power law relation of the diffusivity coefficient $\mathcal{D}$ to $\partial\bar{\theta}/\partial y$ and $\partial\bar{\theta}/\partial p$ of the diffusivity coefficient, we simply assume it to be a constant and use the vertically integrated mean gradient for the parameterization, thus

$$\left(\overline{v'\theta'}\right)_{p_{560}} \sim -\mathcal{D}\left\langle\frac{\partial\bar{\theta}}{\partial y}\right\rangle, \tag{5}$$

where the angle bracket denotes vertical integration over the troposphere (from surface to tropopause). This simple relation turns out to be a better fit to the model results than more nuanced choices of diffusivity parameterization (such as those in Green (1970), Stone (1972), Held (1978a), and Branscome (1983)); it also gives rise to the best theoretical scaling based on a

static stability theory later in Section 5b. It is beyond the scope of the present study to understand why relationship (5) works best for the eddy heat flux in moist models, a topic we leave for future investigation.

Further, using the tropospherically averaged stratification as an approximation for that at the mid-troposphere (560hPa) and substituting (5) into (4), we obtain

$$\mathcal{H}_2 \propto -f \left\langle \frac{\partial \bar{\theta}}{\partial y} \right\rangle \left\langle -\frac{\partial \bar{\theta}}{\partial p} \right\rangle^{-1}, \tag{6}$$

in which the modulating effect of the factor $1/p_s$ on the meridional structure of $\mathcal{H}_2$ has been neglected and the variation with latitude of the Coriolis parameter *f* is also considered. We denote the right hand side of (6) as ξ. ξ measures approximately the isentropic slopes in a vertically averaged sense, which is also an indicator for baroclinicity. If this simple parameterization is valid, one should expect the axis of the storm track/EDSW to vary in concert with the maximum of ξ. This is largely the case for the simulations with both the idealized and full models (see Figure 8a for the idealized model simulations). Choosing the central case in Figure 2, i.e., [T_m=20°C, ΔT=40°C], as the reference state, and using y_0 to denote the reference location of the EDSW, we observe from the modeling results that the peak profiles of the EDSW are shaped by that of the ξ near y_0 for cases neighboring the reference state, or mathematically,

$$\partial \ln U / \partial y \sim \partial \ln \xi / \partial y \quad \text{near } y_0 . \tag{7}$$

In discrete form (7) becomes

$$\frac{U^+ - U^-}{U_m} \sim \frac{\xi^+ - \xi^-}{\xi_m} \quad \text{near } y_0 . \tag{7'}$$

Here, *U* indicates the EDSW; the superscript + (-) denotes a latitudinal average over the polar (equatorial) flank of the reference latitude y_o (see Appendix A); subscript *m* indicates the

maximum value near y_o. In practice, we choose two latitudinal bands, [27°-47°] and [47°-67°], centered around $y_o = 47°$. This is equivalent to discretizing (7) on a coarse 20° grid. Differential perturbations of the wind speed on either sides of y_o should lead to a shift, which, with the aid of a Taylor series expansion, can be expressed as

$$\delta y \approx \frac{U_{rm}}{U_{pm}} \cdot \left(\delta U^{+} - \delta U^{-} \right) \cdot \left\{ \left[\frac{dU_r}{dy} \right]^{-} - \left[\frac{dU_r}{dy} \right]^{+} \right\}^{-1}, \tag{8}$$

where, U_r and U_p are the reference and perturbed surface wind, respectively; $\delta U^{+(-)}$ is the wind perturbation averaged within the [47°-67°] ([27°-47°]) latitudinal band with δ indicating the difference from the reference value. In deriving (8), an assumption has been made to the perturbed wind that the shape of the jet remains to be the same and only the position and the amplitude are altered. As a result, the shift of the jet under perturbations in both the latitude and the amplitude is not only proportional to the differential wind change, but also inversely proportional to the amplitude of the perturbed wind.

Insofar as the perturbation is not too large to invalidate the relation (7'), one may substitute (7') into (8) for both the reference wind and the perturbation wind and obtain a proportional relationship between the shift of the EDSW and the fractional differential change of ξ

$$\delta y \propto \frac{\delta \xi^{+} - \delta \xi^{-}}{\xi_{pm}}. \tag{9}$$

Relation (9) implies that the EDSW tends to shift towards the side of the jet where baroclinicity is enhanced and move away from the side where baroclinicity is reduced, just as shown in the studies of Chen et al. (2010) with varying the sign and the latitude of the gradient of SST perturbations in a similar aquaplanet setting and of Ring and Plumb (2008) with a dry dynamical

core. Readers are referred to Appendix A for the details of the derivation of (8) and (9). The way this relation is derived renders itself to have a limited validity for small perturbation about the reference state. However, to test the limit of it, we examine the right hand side of (9) for all the cases.

5. Validation

5a. Relationship (9) based on model simulations

Figure 4 shows how well the relationship (9) holds for the idealized model between the fractional differential changes of ξ estimated from the model-simulated mean temperatures and the variation in the position of the EDSW (the total value is used). A qualitatively very similar result is found from the full model simulations, and thus not shown. Note that the result of Figure 4 is not very sensitive to which exact pixel point around (T_m =20, ΔT=40) in the T_m -ΔT space is chosen for the reference state. Although linearity does exist in general, it holds best for the cases neighboring the reference state, as highlighted by the circles in Figure 4, but starts to deteriorate when (T_m, ΔT) values deviate markedly from the reference value. However, it is still encouraging to see that the scaling relationship (9) is valid for perturbations in both T_m and ΔT as long as they are small. While this result should not be taken as evidence for the predictive power of equation (9) since ξ is estimated from the model simulations, this corroborates the anticipated connection between the differential change of baroclinicity (and hence the upward eddy EP fluxes) and the shift of the eddy-driven wind. For example, if the baroclinicity increases on the poleward side of the storm track relative to the equatorward side, the source of the baroclinic wave activity shifts poleward. Consequently, the divergent wave propagation in the upper troposphere, which

corresponds to convergence of eddy momentum flux, should shift poleward accordingly, driving a poleward shift of the EDSW through momentum balance.

We next examine how ξ and its components, i.e., the static stability and the tropospheric temperature (meridional) gradient, vary under each SST condition. Figure 5 shows the profiles of ξ in the idealized simulations broken down into different ΔT groups. Overall, the magnitude of ξ increases with ΔT (with an intriguing exception for T_m=0 wherein the midlatitude static stability increases at a greater rate than the tropospheric temperature gradient with increasing ΔT), and decreases substantially with T_m owing to the increase of static stability. A similar tendency is also found in the simulations with the full GCM. As a result, the mid-latitude isentropic slope flattens considerably with increasing T_m, in contrast to the constant isentropic slopes as rationalized from the arguments of baroclinic adjustment (Stone, 1978; Stone and Nemet, 1996) or neutral supercriticality owing to weak nonlinearity in the atmospheric eddy-eddy interactions (Schneider and Walker, 2006). This result suggests that the existing dry theories for the midlatitude adjustment are inadequate to describe the mid-latitude tropospheric thermal stratification under large SST boundary perturbations, as least for these idealized experiments examined here (see also Juckes, 2000; Frierson, 2008). In the meantime, the flattening of the isentropic slope with increasing mean temperature is consistent with previous studies on the effects of moisture on baroclinic eddies (Stone and Yao, 1990; Held, 1978b; Gutowski et al., 1992). For example, Held (1978b) studied the effect of adding hydrological cycle to a dry two-layer climate model, and calculated the ratio of the vertical eddy heat flux, weighted by the static stability, to the meridional eddy heat flux weighted by the meridional gradient of potential temperature—a ratio that approximates the mixing slope divided by the isentropic slope. Held found that this ratio was 0.55 in the dry model, close to the value given by classical theories of

baroclinic instability, but increased to 0.90 in his moist case. The increase of the ratio of the mixing slope with respect to the mean isentropic slope was also found in Gutowski et al. (1992) to be the key effect of condensation in the life cycle of mid-latitude eddies. Given the fact that vertical transport of dry static energy by eddies ($\overline{w'\theta'}$) counters the background gradient ($\partial\overline{\theta}/\partial z$), it is conceivable that the increase of mixing slope may contribute to the flattening of the isentropic slope as the uniform SST warming increases moisture content. The involvement of moisture turns the maintenance of the midlatitude mean thermal structure into an issue of three-way interplay among (i) the horizontal eddy heat flux; (ii) the vertical eddy heat flux; and (iii) the eddy-related diabatic heating, and thus posing a challenge for theoretical understanding.

The most prominent aspect of the static stability is its increase with T_m as shown in Figure 6 for the idealized model (see also Frierson, 2008). A qualitatively similar result is also found for the full model. The increase is most prevalent in the tropics, where the vertical thermal profile approximately follows the moist adiabat. The increase also spreads poleward outside of the territory controlled by Hadley cell. From the coldest to the warmest T_m case, the average static stability near the edge of the Hadley cell or the equatorward flank of the reference storm track increases by a factor of 8 (see Figure 9). For each ΔT group, the static stability increases preferentially over the subtropical latitudes relative to higher latitudes as T_m increases, pushing the peak of ξ poleward, a phenomenon that is typical of the response to the GHG induced global warming (Frierson, 2006; Lu et al., 2008; Yin, 2005).

The tropospheric temperature gradients in the simulations are depicted in Figure 7, together with the SST gradient (black curves). For the warm T_m cases, the gradient profiles exhibit two peaks, a subtropical one associated with the thermally-forced subtropical jet (a same suite of simulations running on an axisymmetric, eddy-free configuration elucidate unambiguously the

subtropical peak, not shown), and a subpolar one associated with the eddy-driven jet. For the moderate and weak T_m cases, these two peaks are merged and indistinguishable. If one defines the edge of the Hadley cell as the subtropical peak of the temperature gradient, the width of the Hadley cell can hardly exceed 35° latitude, in accordance with the notion that the meridional scale of the Hadley cell is set by the location where the thermally driven subtropical jet first becomes baroclinically unstable (Held, 2000; Lu et al., 2007; Frierson et al., 2007b). However, the location of the EDSW associated with the eddy momentum convergence varies over a much wider range between 30° and 65° latitude (see also Figures 1 and 3). It is particularly notable that, for the cases with large T_m and ΔT, the EDSW maximum and the associated maximum temperature gradient are located significantly poleward of the maximum SST gradient (located at 45° for all cases). This poleward enhancement of the gradient reflects the notion of a self-maintaining eddy-driven jet: a self-maintaining jet preserves and sometimes reinforces the mid-latitude gradient and places the gradient on the poleward side of the imposed baroclinicity through the Transformed Eulerian Mean overturning circulation (Robinson, 2000; 2006; Chen and Plumb, 2009). The creation of baroclinicity in the life cycle of eddies has also been explicitly demonstrated in the seminal work of Simons and Hoskins (1978) and Hoskins (1983).

The self-maintaining nature of the EDSW poses a challenge for us to predict the storm track or jet position based on the atmospheric temperature gradient, since itself is largely the result of the baroclinic eddy adjustment. It may be more desirable to predict the location of the storm track using the baroclinicity estimated from the temperature of the axisymmetric, eddy-free simulations, and in this approach the effects in both static stability and tropospheric temperature gradient of eddy adjustment are excluded from the predicting factors. However, the evaluation of ξ using the axisymmetric simulations turns out to be fruitless. Figure 8ab contrasts the locations

of the maximum baroclinicity ξ estimated from the original, eddy-permitted simulations and the eddy-free simulations by the same idealized model, and their alignment/misalignment with locations of the storm tracks. While ξ from the original simulations serves as a good indicator of the axis of the storm track, ξ from the eddy-free simulations just scatters between 50° and 60° latitude and shows little agreement with the storm track locations. It even fails to shift poleward with increasing T_m — the most robust behavior of the storm track in all our eddy-permitted model simulations. As a result, the baroclinicity from the eddy-free state provides almost no clue as to which way the storm track should shift. This could be partly due to the specific prescriptions of the SST conditions, of which the maximum gradients are always fixed at 45° latitude. On the other hand, the variation of static stability, to the extent that it can be predicted solely from the information of SST regardless of the position of the storm track, as will be demonstrated next, may be of some guiding value regarding the shift of the storm track and the tropospheric temperature gradient.

5b. Implication from a static stability theory

Here we estimate $\frac{\delta\xi^{+} - \delta\xi^{-}}{\xi_{pm}}$ making only use of the variation of static stability, which is predicted based on the theory of Juckes (2000) from the given SST boundary conditions. Note that, unlike the estimation in Section 5a, no information of the simulated atmospheric temperature is used except that of the reference state.

To determine the static stability from the SSTs, we implement the formulation of Frierson (2006, 2008), a variant of the original mechanism proposed by Juckes (2000) for the mid-latitude moist stability, which advocates the importance of (moist) convective baroclinic eddy adjustment

in the establishment of the midlatitude static stability. This theory relates the bulk moist stability $\Delta_z \overline{\theta}_e \equiv \theta^*_{et} - \theta_{es}$, defined as the difference between the near-tropopause saturation equivalent potential temperature and the equivalent potential temperature near surface (with * indicating saturation, and subscripts *t* and *s* tropopause and surface, respectively), to the meridional gradient of surface equivalent potential temperature through a mixing length closure:

$$\theta^*_{et} - \theta_{es} \sim L \partial_y \theta_{es} , \qquad (10)$$

where *L* can be interpreted as the typical meridional extent of the storms. This relation may be intuitively interpreted from a Lagrangian perspective: in midlatitude cyclones, the air mass that convects to the tropopause and sets the value of the tropopause moist static energy (and hence the local moist static stability) has its origin from some distance equatorward ($\overline{\theta}^*_{et} = \overline{\theta}^{eq}_{es}$) via poleward advection of moist and warm air in warm fronts (Pauluis et al., 2008; Pauluis et al., 2010). $\overline{\theta}^{eq}_{es}$ is usually larger than the in situ $\overline{\theta}_{es}$ because for the mean condition, the air masses at lower latitude are usually warmer and moister. The efficiency of the cyclones in tapping in air with high moist static energy from lower latitudes is proportional to its (i) meridional span (this is how the spatial scale L comes in) and (ii) meridional gradient of the surface equivalent potential temperature $\Delta_y \theta_{es}$, with larger gradient sustaining more vigorous eddy advection. If one keeps the spatial scale *L* fixed for different SST boundary conditions, as practiced in this scaling study, this is tantamount to fixing the moist isentropic slope $L \sim \Delta_z \overline{\theta}_e / \Delta_y \overline{\theta}_{es}$ over the eddy-dominant latitudes.

Here for our specific purpose of scaling, we predict the (dry) bulk static stability, which is defined as the potential temperature difference between the tropopause and the surface, and averaged over the 30°-50° latitudinal band (on the equatorward flank of the reference EDSW

position), i.e., $\overline{\Delta}_v \equiv \overline{\theta}_t - \overline{\theta}_s$, with the overbar indicating the latitudinal average. To proceed, first we evaluate the right hand side of (10) approximately by the surface equivalent potential temperature difference between 30° and 50° (this is equivalent to fixing *L* in (10)). Thus the average bulk moist stability over this 20°-wide latitudinal band can be approximated as $\Delta_z \overline{\theta}_e \sim \theta_{es}^{30^\circ} - \theta_{es}^{50^\circ}$. Adding it onto the surface equivalent potential temperature ($\overline{\theta}_{es}$), which is computed from the averaged SST over 30°-50° assuming constant relative humidity 0.8, we then obtain the near-tropopause level (300 hPa is actually used) saturation equivalent potential temperature $\overline{\theta}_{et}^* \sim \overline{\theta}_{es} + (\theta_{es}^{30^\circ} - \theta_{es}^{50^\circ})$ wherein the definition of the bulk moist stability has been used. Finally, the upper level potential temperature $\overline{\theta}_t$ over the 30°-50° band can be retrieved through the relationship between potential temperature and saturated equivalent potential temperature at the given pressure (300 hPa). The resultant estimate of the subtropical bulk static stability ($\overline{\Delta}_v$) is shown to be in excellent agreement with the actual simulations (see Figure 9). The choice of the 300 hPa level instead of using the actual tropopause level is simply because, for one reason no theory exists that can predict the tropopause height accurately based on the SST; for another the tropopause pressure in the idealized model is insensitive to the surface temperature, as noted in Frierson (2008). Thus, as a first order approximation it may be justifiable to use a constant pressure level for the tropopause in this simple scaling.

In view of the fact that the static stability does not vary as much over the poleward side as compared with the equatorward side of the jet (Figure 6), we neglect the change in $\delta\xi^+$ and approximate $\delta\xi^-$ with a theoretical estimate $\delta\xi_t^-$ (with subscript *t* indicating theoretical

estimation) in the evaluation of $\frac{\delta\xi^+ - \delta\xi^-}{\xi_{pm}}$. As such, $\frac{\delta\xi^+ - \delta\xi^-}{\xi_{pm}}$ is simplified to be $-\frac{\delta\xi_t^-}{\xi_{pm}}$. In estimating $-\frac{\delta\xi_t^-}{\xi_{pm}}$, the temperature gradient component of $\delta\xi_t^-$ is fixed at the reference value and theoretical estimates at the equatorial flank of the jet are used for the static stability part in $\delta\xi_t^-$; ξ_{pm} is approximated by an average between the reference value at the poleward flank of the jet (which is therefore fixed) and the theoretically estimated value at the equatorward flank of the jet (which varies with SSTs). The result is presented in Figure 10 for the idealized model, showing a tight relationship between the quantity $-\frac{\delta\xi_t^-}{\xi_{pm}}$ and the axis of the EDSW/storm track. The extended good linear fit to the large perturbation cases is not expected, and should be interpreted with caution. In fact, when the baroclinicity changes (due to temperature gradients and/or static stability) on the poleward of the reference jet are taken into consideration, the linear fit deteriorates towards the situation as depicted in Figure 4. One obvious reason, but not the only reason, is that for the wide range of variation of the westerly jet/storm track positions between 30° and 60° latitude, many may violate the constraint of small perturbations with respect to the 47° latitude reference jet position. Nevertheless, the overall results of this scaling effort corroborate the notion that eddy activity and the eddy-induced wind do feel the changes in subtropical static stability, with an increase in the latter causing a poleward shift of the former. Quantitatively, a unit (or 100%) increase in $-\frac{\delta\xi_t^-}{\xi_{pm}}$ can lead to ~7° shift of the EDSW/storm track.

A dynamical scaling that works would hopefully be only weakly dependent on the model configuration. Thus, to assess model dependency, we apply this same scaling to the simulations with the full GCM over the similar suite of SST boundary conditions. The result for all the cases turns out to be a significant deviation from a linear relationship (Figure 11a), confirming our suspicion that the linearity between $-\frac{\delta\xi_t^-}{\xi_{pm}}$ and the EDSW shift for large perturbation cases in the idealized model may be fortuitous. This may also be due to the regime behavior of the position of the EDSW over the wide range of ΔT as discussed in Section 3. Indeed, when applying the scaling to the T_m-ΔT domain wherein the wind profiles are characteristic of single-jet and the EDSW shows a monotonic relationship to both T_m and ΔT, the linear relationship between $-\frac{\delta\xi_t^-}{\xi_{pm}}$ and the actual shift resumes (Figure 11b). It is especially encouraging to note that the slope of the linear relationship in Figure 11b is very similar to that in the idealized model — ~6° shift for per unit increase of $-\frac{\delta\xi_t^-}{\xi_{pm}}$. In summary, the simple static stability-based scaling has shown to be valid and robust in the shift of the EDSW/storm track simulated by two rather different aquaplanet GCMs, insofar as the wind profile resides in a same dynamic regime and the SST perturbations are not so large as to cause wind regime transitions.

6. Summary and concluding remarks

The midlatitude storm track shifts poleward in simulations for the 3rd Coupled Model Intercomparison Project (CMIP3) under the GHG-induced global warming. No widely accepted theory exists to rationalize this phenomenon, except that some studies suggest that it links to the

rise of the tropopause (Williams, 2006; Lorenz and DeWeaver, 2007) and the attendant eddy feedbacks through the eddy phase speed changes (Chen and Held, 2007; Chen et al., 2008; Lu et al., 2008). Here, by diagnosing a suite of aquaplanet simulations with two distinct GCMs under specified SST boundary conditions, we demonstrate that the variation of the zonal index (or the shift of the surface westerly winds) can be thought of as being constrained by the structure of the lower tropospheric Eliassen-Palm activity flux (predominantly the heat flux) coming out of the lower troposphere. The latter, parameterized as a quantity measuring the tropospheric baroclinicity, shows a strong sensitivity to the perturbation in the subtropical static stability. In both an idealized GCM and a GCM with full physics, the preferential stabilization at the equatorial flank of the storm track/EDSW can, at least within the climate regime similar to the present climate in the Northern Hemisphere winter, shift poleward the baroclinicity and hence the production of the eddy activity flux. Since the source of the horizontal eddy activity flux (equivalent to the convergence of eddy momentum flux) in the upper troposphere determines the position of the EDSW through the momentum balance upon vertical integration, a poleward displacement of the source of the eddy activity flux heralds a poleward shift of EDSW. Through this chain of reasoning, the displacement in the position of EDSW may be predictable provided the information of static stability can be derived exclusively from the given SST conditions. Finally, a good relationship results between the static stability-based estimation of baroclinicity and the position of EDSW in both the idealized and the full GCMs, suggesting the importance of static stability as a key dynamical factor for understanding the shift of storm track and the associated eddy-mean flow interaction.

This assertion should not be confused with the scaling theory for the width of the Hadley cell advocated by Frierson et al. (2007), wherein the subtropical static stability has been found to

scale with the Hadley cell width in the same aquaplanet simulations examined here (see their Figures 1 and 2). We stress the distinction between the scaling for the Hadley cell width and the scaling constructed here for the storm track position: the static stability in the former acts on the subtropical baroclinicity associated with the thermally forced subtropical jet within the Hadley cell while in the latter through the midlatitude baroclinicity to influence the storm track. Moreover, the Hadley cell width scaling is much less susceptible to the jet regime transition as one can discern from inspecting Figure 1ab here and Figure 1 in Frierson et al. (2007).

The importance of static stability in the shift of storm track and EDSW is further corroborated by the analysis of the simulations by the state-of-the-art CMIP3 models: as one can infer from Figure 6b in Lu et al. (2008), the models with greater increase in static stability to the immediate equatorward side of the storm track tends to show a larger poleward displacement of EDSW. In the meantime, the scaling put forward in this study should not be considered contradictory, but complementary to the mechanism proposed by Lorenz and DeWeaver (2007) for the case of global warming, which emphasizes the role of the tropopause rise. The rise of tropopause is associated with an upper tropospheric warming and a stratospheric cooling under the direct and indirect effect of the greenhouse gas forcing; they can modulate the upper tropospheric wave propagation and eddy momentum flux, and consequently the position of the eddy driven westerly wind (Chen et al. 2007; Chen and Held, 2007; Chen et al., 2008). The relative contributions to the EDSW shift from the mechanism of static stability versus that of tropopause rise remain to be quantified, a topic of our ongoing investigation.

The anomaly-wise scaling proposed here is shown to be valid for perturbations in both the global mean and the equator-to-pole gradient of the SST up to an order of 10 K, it thus may have some implications on the change of the storm track during the past of the Earth's climate. For

example, during the glacial periods when the global mean temperature was about 10 K cooler than the present, our scaling would suggest the storm track should be several degrees equatorward relative to today. This speculation is consistent with the higher-than-today loading of mineral dust from ice core records (e.g., Petit et al., 1999), attributable to the larger exposure of the subtropical desert to the uplift by midlatitude storm systems as they retreat equatorward in a colder climate (Chylek et al., 2001). For another application, during the mid-Holocene (about 6000 yrs ago), the solar radiation in the Southern Hemisphere had a weaker equator-to-pole gradient during the austral spring followed by an overall dimming during summer, which could conceivably lead to an equatorward movement of the austral summer storm track. Whether this is true remains to be verified by paleoclimatic data.

Acknowledgements

The perceptive and constructive comments from Paul O'Gorman and other two anonymous reviewers have dramatically improved the clarity of the manuscript. We also thank David Straus for his internal review at COLA. JL is supported by the startup fund at George Mason University and the COLA omnibus fund from NSF grant 830068, NOAA grant NA09OAR4310058, and NASA grant NNX09AN50G. GC is supported by the startup fund at Cornell University. DMF is supported by NSF grants ATM-0846641 and AGS-0936069.

Appendix A: Formulation of shift

Empirically speaking, dipolar wind anomalies centered about the axis of a jet can lead to a shift of the jet. Here, we derive a functional relationship between the shift of the jet and the dipolar wind anomalies considering perturbations in both latitudinal position and the magnitude of the jet but with the shape kept the same.

We denote the reference and perturbed wind profiles as U_r and U_p, respectively, and the corresponding maximum of the jet as U_{rm} and U_{pm}. The perturbed wind U_p is shifted meridionally by δy and amplified by a factor of $1+\alpha$ with respect to the reference wind, while maintaining the same structure as the reference wind, therefore, $U_p(y) = (1+\alpha)U_r(y-\delta y)$. With the aid of a Taylor expansion, the difference between U_p and U_r can be expressed as

$$\begin{aligned}
\delta U &\equiv U_p - U_r \\
&= (1+\alpha)U_r(y-\delta y) - U_r(y) \\
&= (1+\alpha)\left\{U_r(y) - \frac{dU_r}{dy}\cdot\delta y\right\} - U_r(y) \\
&= \alpha U_r(y) + (1+\alpha)\left\{-\frac{dU_r}{dy}\cdot\delta y\right\},
\end{aligned} \tag{A1}$$

Averaging δU within the two latitude boxes at the flanks of the reference jet and taking the difference yields

$$\delta U^+ - \delta U^- = \alpha\left[U_r\right]^+ - \alpha\left[U_r\right]^- + (1+\alpha)\delta y\cdot\left\{\left[\frac{dU_r}{dy}\right]^- - \left[\frac{dU_r}{dy}\right]^+\right\}$$

The two latitude boxes are chosen in such a way that the average of the reference wind within the two boxes is similar, therefore,

$$\delta U^+ - \delta U^- \approx (1+\alpha)\left\{\left[\frac{dU_r}{dy}\right]^- - \left[\frac{dU_r}{dy}\right]^+\right\}\cdot\delta y \tag{A2}$$

Finally, the shift of the jet is related to the dipolar anomalies and the amplification factor as

$$\delta y \approx \frac{\delta U^+ - \delta U^-}{1+\alpha} \cdot \left\{ \left[\frac{dU_r}{dy} \right]^- - \left[\frac{dU_r}{dy} \right]^+ \right\}^{-1},$$

or

$$\delta y \approx \frac{U_{rm}}{U_{pm}} \cdot \left(\delta U^+ - \delta U^- \right) \cdot \left\{ \left[\frac{dU_r}{dy} \right]^- - \left[\frac{dU_r}{dy} \right]^+ \right\}^{-1} \qquad \text{(A3)}$$

With the reference state chosen, the term in brackets is a constant, thus we yield a proportionality relation

$$\delta y \propto \frac{U_{rm}}{U_{pm}} \cdot \left(\delta U^+ - \delta U^- \right) = U_{rm} \cdot \left\{ \frac{(U_p^+ - U_p^-) - (U_r^+ - U_r^-)}{U_{pm}} \right\} \qquad \text{(A4)}$$

To relate the shift of wind to the differential change of the baroclinicity ξ, we substitute (7') into (A4) and make use of another assumption that fractional change of the peak wind speed is proportional to that of the baroclinicity, i.e., $\frac{U_{rm}}{U_{pm}} \sim \frac{\xi_{rm}}{\xi_{pm}}$, which is a reasonable first order approximation to the actual model simulations. The result is simply the proportionality relation (9).

References

Bengtsson, L., K. I. Hodges, and E. Roeckner, 2006: Storm tracks and climate change, *J. Climate*, **19**, 3518–3543.

Betts, A. K., 1986: A new convective adjustment scheme. Part I: Observational and theoretical basis, *Q. J. R. Meteorol. Soc.*, **112**, 677–692.

Betts, A. K., and M. J. Miller, 1986: A new convective adjustment scheme. Part II: Single column tests using GATE wave, BOMEX, and arctic air-mass data sets, *Q. J. R. Meteorol. Soc.*, **112**, 693–709.

Blackmon, M. L., 1976: A climatological spectral study of the 500 mb geopotential height of the Northern Hemisphere. *J. Atmos. Sci.,* **33,** 1607–1623.

Blackmon, M. L., J. M. Wallace, N.-C. Lau, and S. L. Mullen, 1977: An observational study of the Northern Hemisphere wintertime circulation. *J. Atmos. Sci.,* **34,** 1040 –1053.

Brayshaw, D. J., B. Hoskins, and M. Blackburn, 2008: The storm-track response to idealized SST perturbations in an aquaplanet GCM, *J. Atmos. Sci.*, **65**, 2842-2860.

Branscome, L. E., 1983: A parameterization of transient eddy heat flux on a Beta-plane. *J. Atmos. Sci.*, **40**, 2508-2521.

Bretherton, F. P., 1966: The propagation of groups of internal gravity waves in a shear flow. *Quart. J. Roy. Meteor. Soc.,* **92,** 466-480.

Caballero, R., and P. L. Langen, 2005: The dynamic range of poleward energy transport in an atmospheric general circulation model, *Geophys. Res. Lett.*, **32**, L02705, doi:10.1029/2004GL021581.

Chang, E. K. M., 2001: GCM and observational diagnoses of the seasonal and interannual variations of the Pacific storm track during the cool season, *J. Atmos. Sci.*, **58**, 1784-1800.

Chang, E. K. M., S. Lee, and K. L. Swanson, 2002: Storm track dynamics, *J. Climate*, **15**, 2163-2183.

Charney, J. G., 1947: The dynamics of long wave in a baroclinic westerly current. *J. Meteor.,* **4**, 135-162.

Chen, G., I. M. Held, and W. A. Robinson, 2007: Sensitivity of the latitude of the surface westerlies to surface friction. *J. Atmos. Sci.*, **64**, 2899-2915, doi:10.1175/JAS3995.1.

Chen, G., and I. M. Held, 2007: Phase speed spectra and the recent poleward shift of Southern Hemisphere surface westerlies. *Geophys. Res. Lett.*, **34**, L21805, doi:10.1029/2007GL031200.

Chen, G., Lu, J. and D. M. W. Frierson, 2008: Phase Speed Spectra and the Latitude of Surface Westerlies: Interannual Variability and Global Warming Trend. *J. Climate*, **21**, 5942-5959.

Chen, G., and R. A. Plumb, 2009: Quantifying the eddy feedback and the persistence of the zonal index in an idealized atmospheric model. *J. Atmos. Sci.*, **66,** 3707-3719.

Chen, G., R. A. Plumb, and J. Lu, 2010: Sensitivities of zonal mean atmospheric circulation to SST warming in an aqua-planet model. *Geophys. Res. Lett.*, in press.

Chylek, P., G Lesins, and U. Lohmann (2001), Enhancement of dust source area during past glacial periods due to change of the Hadley circulation, *J. Geophys. Res.*, **106**(D16), 18,477-18,485.

Eady, E. T., 1949: Long waves and cyclone waves. *Tellus*, **1**, 33-52.

Edmon H. J. Jr., B. J. Hoskins, and M. E. McIntyre, 1980: Eliassen–Palm cross sections for the troposphere. *J. Atmos. Sci.*, **37**, 2600–2616.

Frierson, D. M. W. (2006), Robust increases in midlatitude static stability in simulations of global warming, *Geophys. Res. Lett.*, **33**, L24816, doi:10.1029/2006GL027504.

Frierson, D. M. W. (2008), Midlatitude static stability and simple and comprehensive general circulation models, *J. Atmos. Sci.*, **65**, 1049-1062.

Frierson, D. M. W., I. M. Held, and P. Zurita-Gotor, 2006: A gray-radiation aquaplanet moist GCM. Part I: Static stability and eddy scale, *J. Atmos. Sci.*, **63**, 2548–2566.

Frierson, D. M. W., I. M. Held, and P. Zurita-Gotor, 2007a: A gray-radiation aquaplanet moist GCM. Part II: Energy transports in altered climates, *J. Atmos. Sci.,* **64**, 1680-1693.

Frierson, D. M. W., J. Lu, and G. Chen, 2007b: The width of Hadley circulation in simple and comprehensive general circulation models. *Geophys. Res. Lett.,* **34**, L18804, doi: 10.1029/2007GL031115.

Green J. S., 1970: Transfer properties of the large scale eddies and the general circulation of the atmosphere. *Quart. J. Roy. Meteor. Soc.*, **96**, 157–185.

Gutowski, W. J., 1992: Life cycles of moist baroclinic eddies. *J. Atmos. Sci.,* **49**, 306-319.

Hartmann, D. L., 1974: Time spectral analysis of mid-latitude disturbances. *Mon. Wea. Rev.,* **102**, 348-362.

Held, I. M., 1978a: The vertical scale of an unstable baroclinic wave and its importance for eddy heat flux parameterizations. *J. Atmos. Sci.,* **35**, 572-576.

Held, I. M., 1978b: The tropospheric lapse rate and climate sensitivity: Experiments with a two-level atmospheric model. *J. Atmos. Sci.,* **35**, 2083-2098.

Held, I. M., and Coauthors, 2000: The general circulation of the atmosphere. *Proc. Program in Geophysical Fluid Dynamics*. Wood Hole, MA. Woods Hole Oceanographic Institute, 1-54. [Available online at http://gfd.whoi.edu.]

Hoskins, B. J., 1983: Modelling of the transient eddies and their feedback on the mean flow. In *Large-scale dynamical processes in the atmosphere*. Eds. B. J. Hoskins and R. P. Pearce.

Academic Press, New York. 169-199.

Hoskins, B. J., H.-H. Hsu, I. N. James, M. Matsutani, P. D. Sardeshmukh, and G. H. White, 1989: *Diagnostics of the Global Atmospheric Circulation Based on ECMWF Analysis 1979-1989*. WCRP-27, WMO/TD-No.326. Available from Joint Planning Staff for the WCRP, c/o World Meteorological Organization, Case Postale No. 2300, CH-1211 Geneva 2, Switzerland.

Hoskins, B. J. and Valdes 1990: On the existence of storm tracks. *J. Atmos. Sci.,* **47**, 1854-1864.

Inatsu, M., H. Mukougawa, and S.-P. Xie, 2003: Atmospheric response to zonal variations in midlatitude SST: Transient and stationary eddies and their feedback, *J. Climate*, **16**, 3314–3329.

James, I. N., 1987: Suppression of baroclinic instability in horizontally sheared flows. *J. Atmos. Sci.*, **44**, 3710-3720.

Jacob, R., 1997: Low frequency variability in a simulated atmosphere ocean system, Ph.D thesis, Univ. of Wis.-Madison. Madison.

Juckes, M. N. (2000), The static stability of the midlatitude troposphere: The relevance of moisture, *J. Atmos. Sci.*, **57**, 3050–3057.

Kiehl, J. T., J. J. Hack, G. B. Bonan, B. A. Boville, B. P. Brieglieb, D. L. Williamson, and P. J. Rasch (1996), Description of the NCAR Community Climate Model (CCM3), *Tech. Rep. TN-420*, Natl. Cent. for Atmos. Res., Boulder, Colo.

Kushner, P. J., I. M. Held, and T. L. Delworth, 2001: Southern Hemisphere atmospheric circulation response to global warming, *J. Climate*, **14**, 2238–2249.

Lee, S., and H.-K. Kim, 2003: The dynamical relationship between subtropical and eddy-driven jets, *J. Atmos. Sci.*, **60**, 1490–1503.

L'Heureux and Thompson, 2006: Observed relationships between the El Niño–Southern Oscillation and the extratropical zonal-Mean circulation *J. Climate*, **19**, 276-287.

Lorenz, D. J., and E. DeWeaver (2007), Tropopause height and the zonal wind response to global warming in the IPCC scenario integrations, *J. Geophys. Res.*, **112**, D10119, doi:10.1029/2006JD008087.

Lu, J., G. Chen, and D. Frierson, 2008: Response of the zonal mean atmospheric circulation to El Nino versus global warming, *J. Climate*, **21**, 5835- 5851, doi:10.1175/2008JCLI2200.1.

Lu, J., G. A. Vecchi, and T. Reichler (2007), Expansion of the Hadley cell under global warming, *Geophys. Res. Lett.*, **34**, L06805, doi:10.1029/2006GL028443.

Nakamura, H. (1992), Midwinter suppression of baroclinic wave activity in the Pacific, *J. Atmos. Sci.*, **49**, 1629-1642.

Orlanski, I., 2005: A new look at the Pacific storm track variability: sensitivity to tropical SSTs and to upstream seeding. *J. Atmos. Sci.*, **62**, 1367-1390.

Pauluis, O., A. Czaja, and R. Korty, 2008: The global atmospheric circulation on moist isentropics. *Science,* **321,** 1075-1078.

Pauluis, O., A. Czaja, and R. Korty, 2010: The global atmospheric circulation in moist isentropic coordinates. *J. Climate*, in press.

Pavan V., and I. M. Held, 1996: The diffusive approximation for eddy fluxes in baroclinically unstable jets. *J. Atmos. Sci.*, **53**, 1262–1272.

Petit, et al., (1999), Climate and atmospheric history of the past 420,000 years from the Vostok ice core, Antarctica. *Nature*, **399**, 429-436.

Phillips, N. A., 1954: Energy transformations and meridional circulations associated with simple baroclinic waves in a two-level, quasi-geostrophic model. *Tellus*, **6**, 273-286.

Ring, M. J. and R. A. Plumb, 2008: The response to a simplified GCM to axisymmetric forcings: application of the fluctuation-dissipation theorem. *J. Atmos. Sci.,* **65**, 3880-3898.

Robinson, W. A., 2000: A baroclinic mechanism for the eddy feedback on the zonal index, *J. Atmos. Sci.,* **57**, 415-422.

Robinson, W. A., 2002: On the midlatitude thermal response to tropical warming. *Geophys. Res. Lett.,* **29**, doi: 10.1029/2001GL014158.

Robinson, W. A., 2006: On the self-maintenance of midlatitude jets. *J. Atmos. Sci.,* **63**, 2109-2122.

Schneider, T., O'Gorman, P. A., and Levine, X., 2010: Water vapor and the dynamics of climate changes. *Reviews of Geophysics,* doi:10.1029/2009RG000302 (In press).

Schneider, T. and C. C. Walker, 2006: Self-organization of atmospheric macroturbulence into critical states of weak nonlinear eddy-eddy interactions. *J. Atmos. Sci.*, **63**, 1569-1586.

Seager, R., N. Harnik, Y. Kushnir, W. Robinson, and J. Miller, 2003: Mechanisms of hemispherically symmetric climate variability. *J. Clim.*, **16**, 2960-2978.

Simons, A. J. and B. J. Hoskins, 1978: The life cycles of some nonlinear baroclinic waves. *J. Atmos. Sci.*, **35**, 414–432.

Stone, P. H., 1972: A simplified radiative-dynamical model for the static stability of rotating atmospheres. *J. Atmos. Sci.*, **29**, 405–418.

Stone, P. H., 1978: Baroclinic adjustment. *J. Atmos. Sci.*, **35**, 561-571.

Stone, P. H. and B. Nemet, 1996: Baroclinic adjustment: A comparison between theory, observations, and models. *J. Atmos. Sci.*, **53**, 1663-1674.

Stone, P. H. and M.-S. Yao, 1990: Development of a two-dimensional zonally averaged statistical-dynamical model. Part III: The parameterization of the eddy fluxes of heat and

momentum. *J. Climate*, **3**, 726-740.

Straus, D. M. and J. Shukla, 1988: A comparison of a GCM simulation of the seasonal cycle of the atmosphere with observations. Part II: Stationary waves and transient fluctuations. *Atmos.-Ocean*, **26**, 575-607.

Williams, G. P., 2006: Circulation sensitivity to tropopause height. *J. Atmos. Sci.*, **63**, 1954-1961.

Yin, J. H. (2005), A consistent poleward shift of the storm tracks in simulations of 21st century climate, *Geophys. Res. Lett.*, **32**, L18701, doi:10.1029/2005GL023684.

Figure Captions

Figure 1 Upper: latitude of EDSW simulated in (a) the idealized and (b) the full GCMs, respectively. In (b), the crosses mark the cases of double-jet condition. Lower: the latitude of the EDSW versus that of the axis of the storm track in (c) the idealized and (d) the full GCMs. The storm track is measured as the vertically integrated EKE. The dots in (c) and (d) are color-coded based on the corresponding T_m.

Figure 2 The profiles of 400 hPa zonal wind in the simulations of the full GCM for the cases of T_m=15°C, ΔT varying from 10 to 50 K at increments of 5 K. The cases identified to be in split-jet regimes in Figure 1b are highlighted by the thick lines.

Figure 3 Profiles of lower-level eddy PV flux $\mathcal{F}_2$ (red) and associated eddy heat flux component $\mathcal{H}_2$ (dashed red), upper-level eddy PV flux $\mathcal{F}_1$ (blue) and associated eddy momentum flux component $\mathcal{M}_1$ (dashed black), and the surface wind U_s (black) in the set of simulations by the idealized model. All the eddy flux terms are normalized by the maximum of $\mathcal{F}_2$ and U_s is normalized by its own maximum.

Figure 4 $\frac{\delta\xi^+ - \delta\xi^-}{\xi_{pm}}$ estimated from model-simulated temperature versus the actual axis of the storm track in the idealized GCM. The circles highlight the cases neighboring the reference state.

Figure 5 Baroclinicity ξ ($m^{-1} s^{-1}$) in the set of simulations by the idealized model, broken down into 6 ΔT groups. Curves in each group/panel are color-coded corresponding to the value of T_m the same way as in Fig. 4.

Figure 6 Same as Fig.5 except for the bulk static stability $\bar{\Delta}_v$ (Kelvin).

Figure 7 Same as Fig.5 except for the tropospheric temperature gradients (K m^{-1}).

Figure 8 Bulk static stability (Kelvin) estimated using the Juckes theory versus that simulated directly by the idealized GCM.

Figure 9 (a) latitude of the max baroclinicity ξ versus the location of the max EKE in the original eddy-permitted idealized GCM; (b) same as (a) but ξ are estimated from the temperature simulated by the axisymmetric version of the idealized GCM. The cases in each panel are color-coded based on the corresponding T_m.

Figure 10 $-\frac{\delta\xi_t^-}{\xi_{pm}}$ versus the displacement of the EDSW in the idealized GCM. The theoretical estimate of $-\frac{\delta\xi_t^-}{\xi_{pm}}$ is not evaluated from GCM mean fields, but rather based on the Juckes theory for the bulk static stability and the meridional temperature gradient fixed at the reference value.

Figure 11 (a) Theoretical estimate of $-\frac{\delta\xi_t^-}{\xi_{pm}}$ versus the displacement of EDSW axes in the full GCM for all cases; (b) same as (a) but only for the cases of $\Delta T \geq 30$°C identified as the single-jet regime. The blue, green, yellow, and red colors represent T_m=10, 15, 20, and 25°C, respectively.

Figure A1 Schematic for the shift of the jet under perturbations in both the position and the amplitude of the jet.

List of Figures

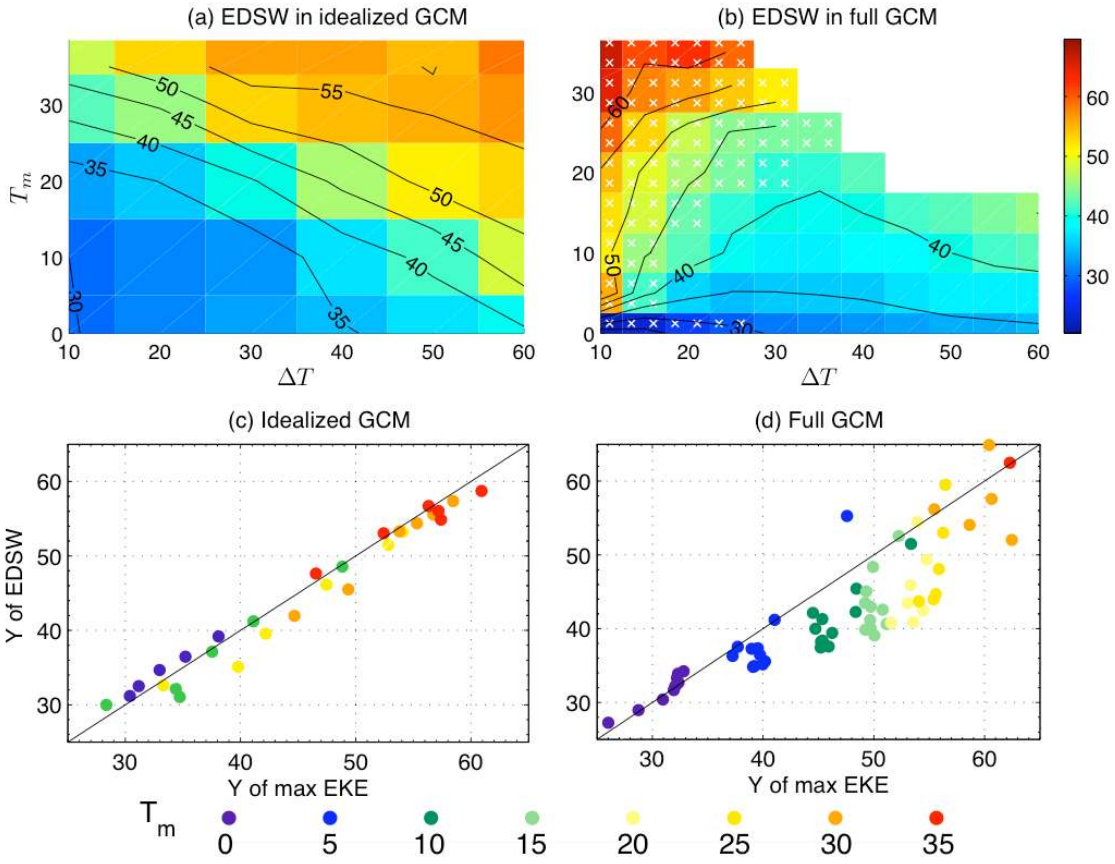

Figure 1 Upper: latitude of EDSW simulated in (a) the idealized and (b) the full GCMs, respectively. In (b), the crosses mark the cases of double-jet condition. Lower: the latitude of the EDSW versus that of the axis of the storm track in (c) the idealized and (d) the full GCMs. The storm track is measured as the vertically integrated EKE. The dots in (c) and (d) are color coded based on the corresponding T_m.

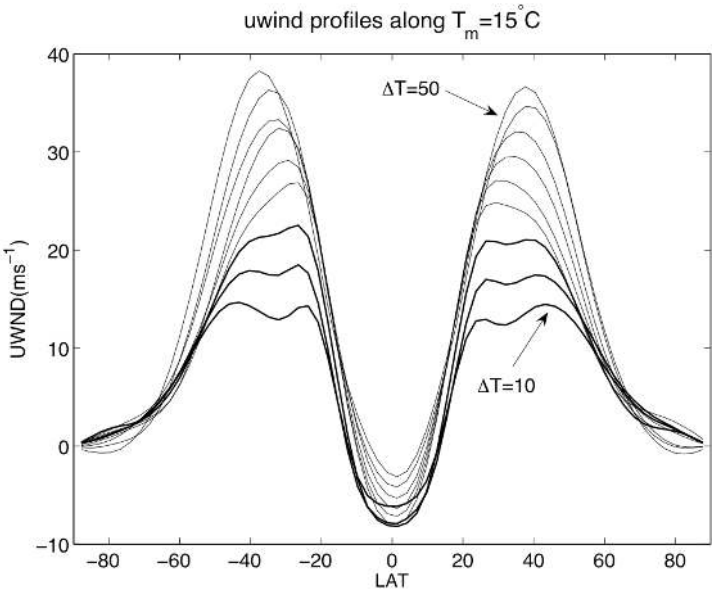

Figure 2 The profiles of 400 hPa zonal wind in the simulations of the full GCM for the cases of T_m=15°C, ΔT varying from 10 to 50 K with increments of 5 K. The cases identified to be in split-jet regimes in Figure 1b are highlighted by thick lines.

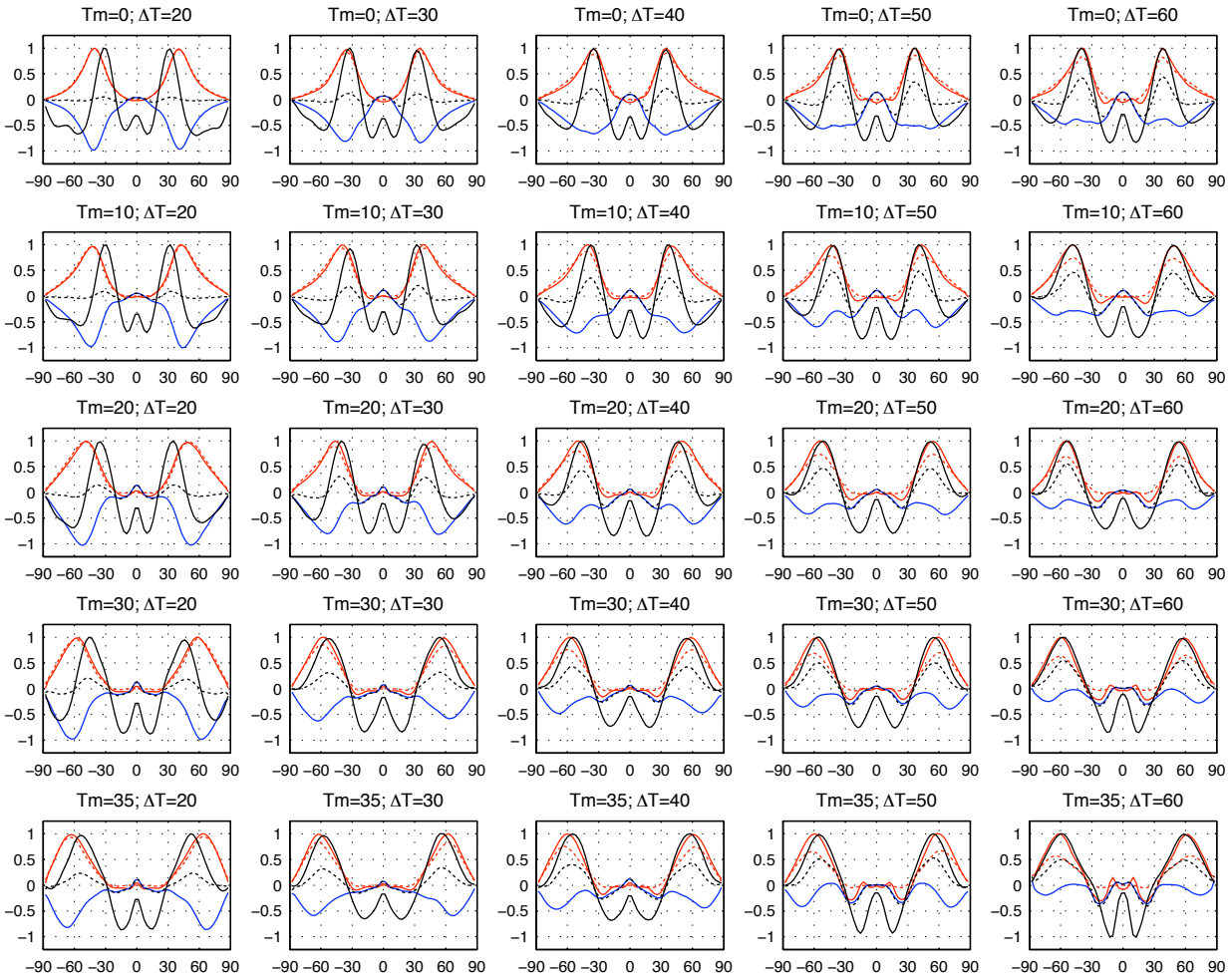

Figure 3 Profiles of lower level eddy PV flux $\mathcal{F}_2$ (red) and associated eddy heat flux component $\mathcal{H}_2$ (dashed red), upper level eddy PV flux $\mathcal{F}_1$ (blue) and associated eddy momentum flux component $\mathcal{M}_1$ (dashed black), and the surface wind U_s (black) in the set of simulations by the idealized model. All the eddy flux terms are normalized by the maximum of $\mathcal{F}_2$ and U_s is normalized by its own maximum.

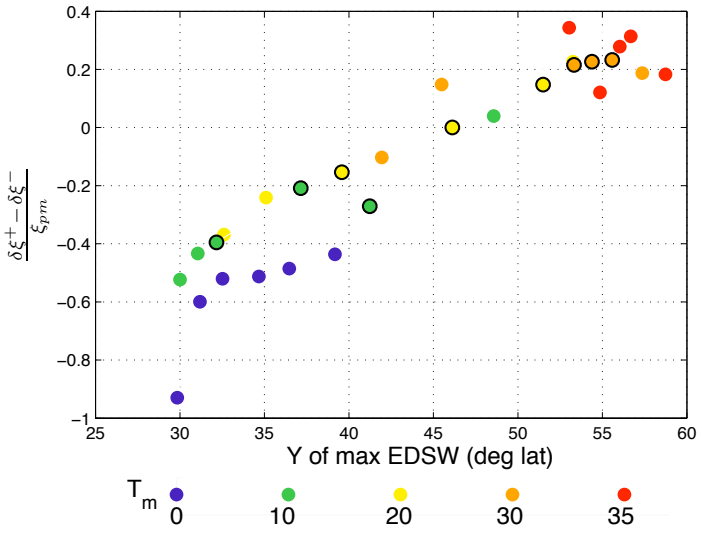

Figure 4 $\frac{\delta\xi^+ - \delta\xi^-}{\xi_{pm}}$ estimated from model-simulated temperature versus the actual axis of the storm track in the idealized GCM. The circles highlight the cases neighboring the reference state. The cases are color-coded based on the corresponding T_m.

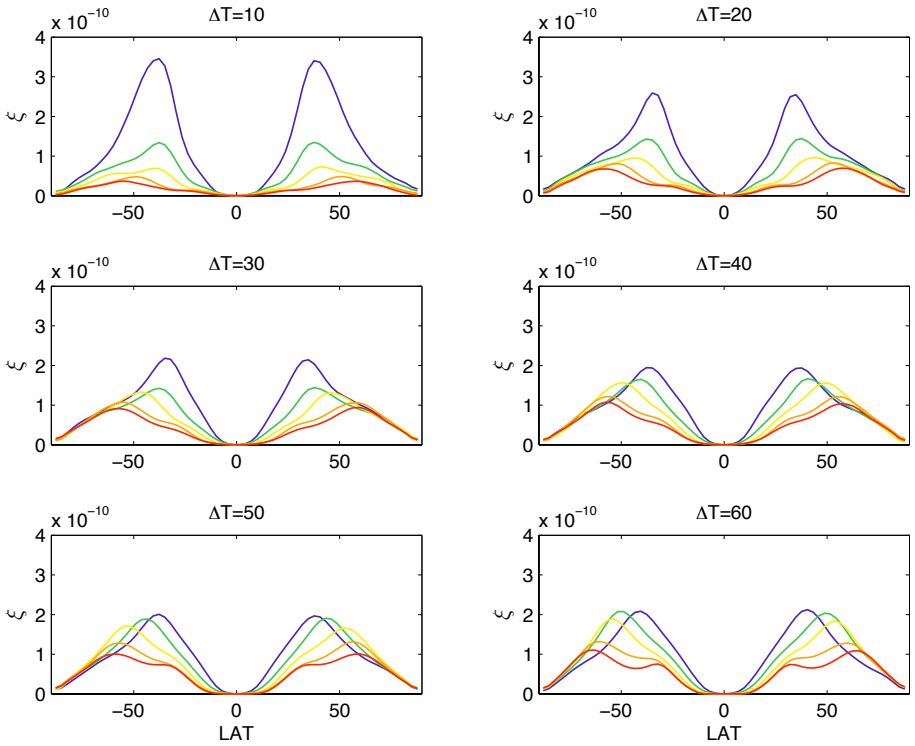

Figure 5 Baroclinicity ξ ($m^{-1} s^{-1}$) in the set of simulations by the idealized model, broken down into 6 ΔT groups. Curves in each group/panel are color coded corresponding to the value of T_m the same way as in Fig. 4.

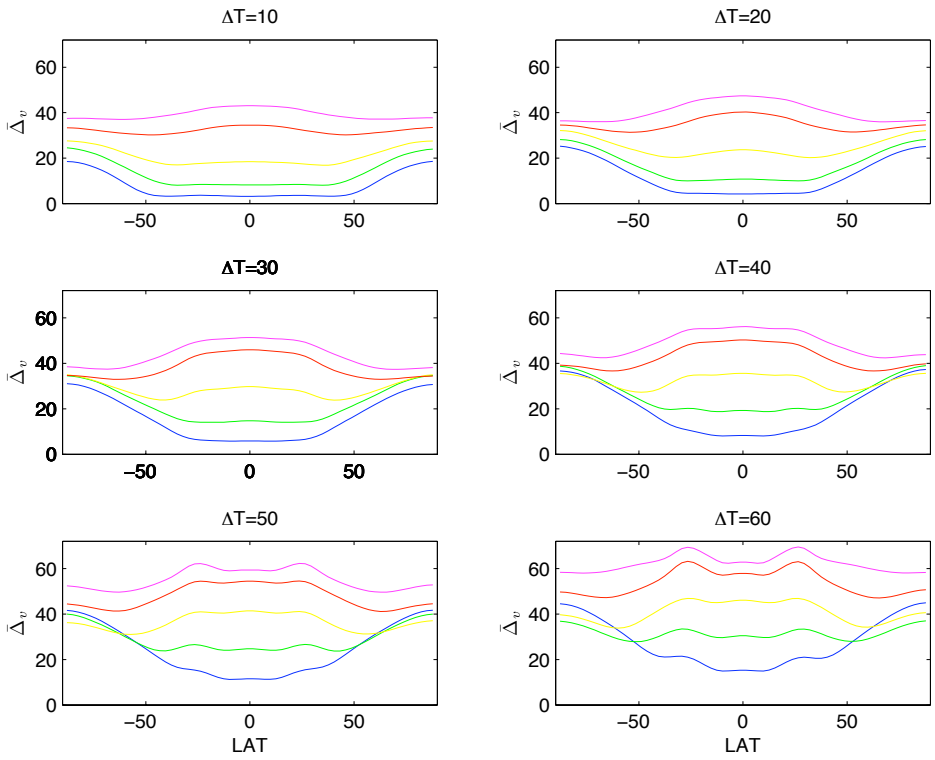

Figure 6 Same as Fig.5 except for the bulk static stability $\bar{\Delta}_v$ (Kelvin).

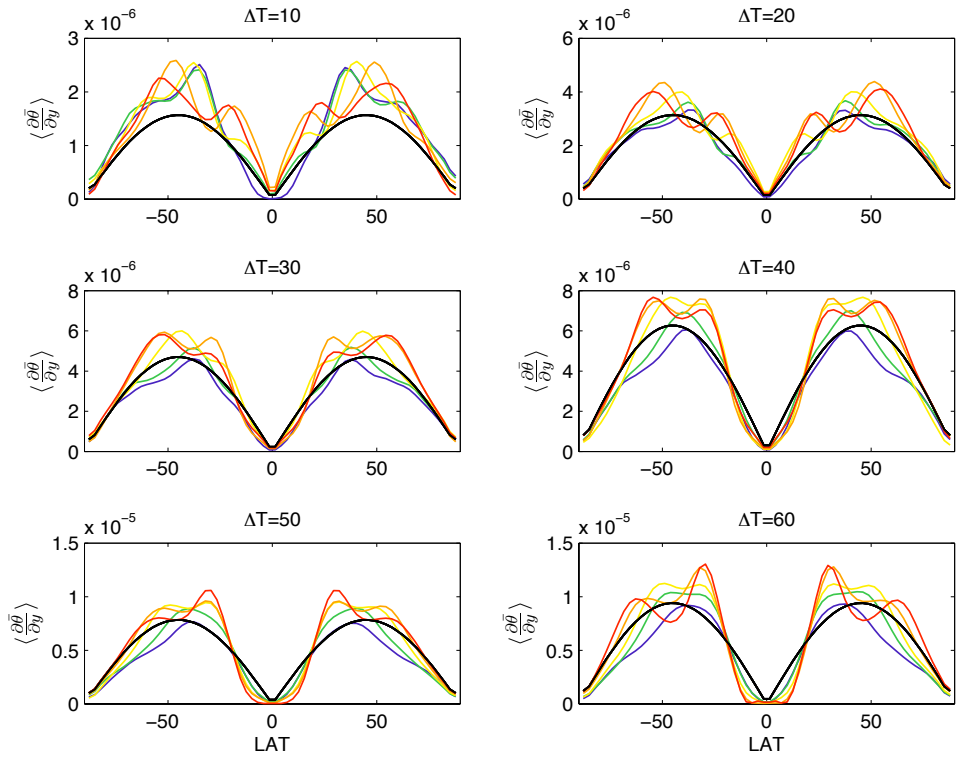

Figure 7 Same as Fig.5 except for the tropospheric temperature gradients (K m^{-1}).

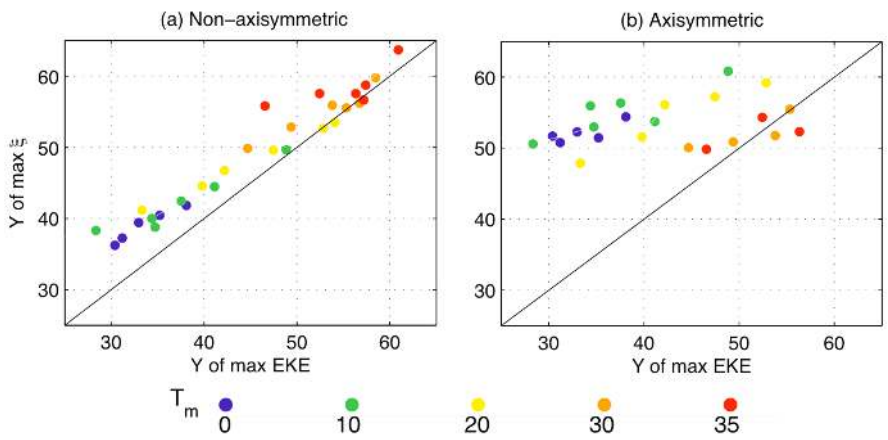

Figure 8 (a) latitude of the max baroclinicity ξ versus the location of the max EKE in the original eddy-permitted idealized GCM; (b) same as (a) but ξ are estimated from the temperature simulated by the axisymmetric version of the idealized GCM. The cases in each panel are color-coded based on the corresponding T_m.

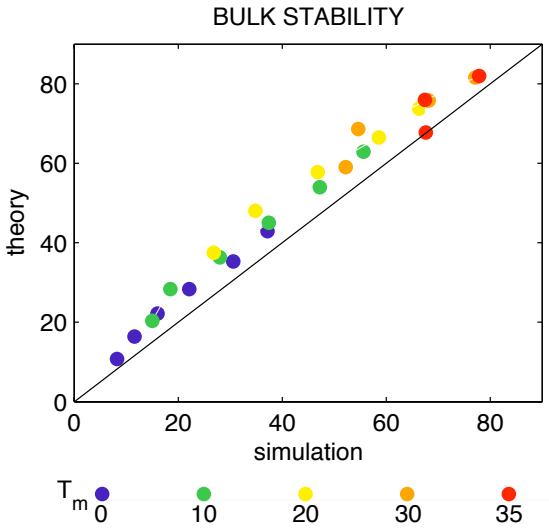

Figure 9 Bulk static stability (Kelvin) estimated using the Juckes theory versus that simulated directly by the idealized GCM.

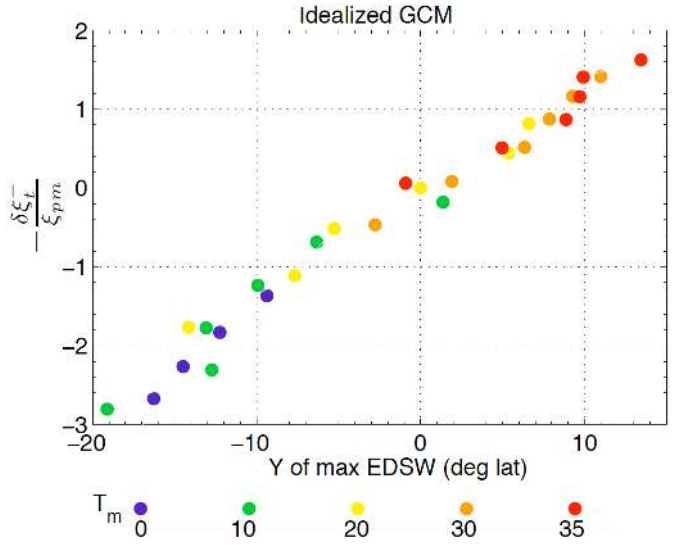

Figure 10 $-\frac{\delta\xi_t^-}{\xi_{pm}}$ versus the displacement of the EDSW in the idealized GCM. The theoretical estimate of $-\frac{\delta\xi_t^-}{\xi_{pm}}$ is not evaluated from GCM mean fields, but rather based on the Juckes theory for the bulk static stability and the meridional temperature gradient fixed at the reference value.

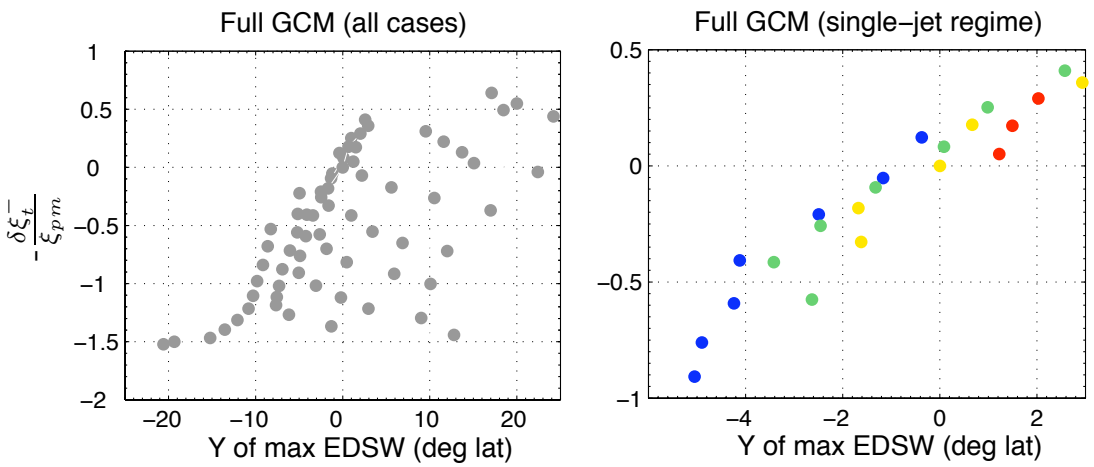

Figure 11 (a) Theoretical estimate of $-\dfrac{\delta\xi_t^-}{\xi_{pm}}$ versus the displacement of EDSW axes in the full GCM for all cases; (b) same as (a) but only for the cases of $\Delta T \geq 30$°C identified as the single-jet regime. The blue, green, yellow, and red colors represent T_m=10, 15, 20, and 25°C, respectively.

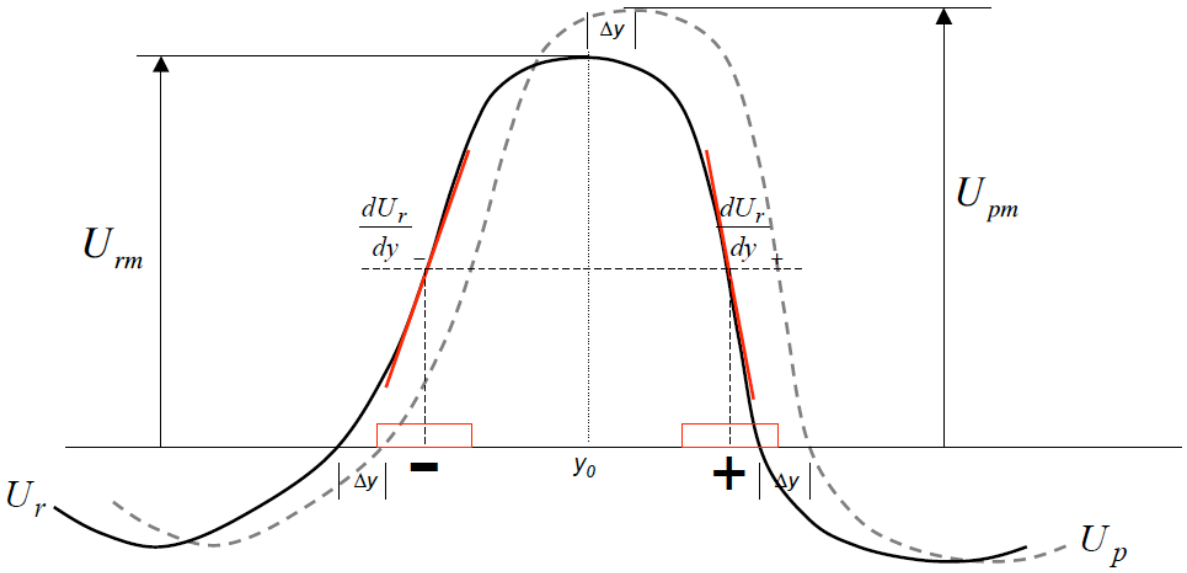

Figure A1 Schematic for the shift of the jet under perturbations in both the position and the amplitude of the jet.